Hidden vortex lattices in a thermally paired superfluid

E. K. Dahl,[1] E. Babaev,[2,3] and A. Sudbø[1]
[1]*Department of Physics, Norwegian University of Science and Technology, N-7491 Trondheim, Norway*
[2]*Department of Physics, University of Massachusetts, Amherst, Massachusetts 01003, USA*
[3]*Department of Theoretical Physics, The Royal Institute of Technology, 10691 Stockholm, Sweden*
(Received 2 September 2008; published 15 October 2008)

We study the evolution of rotational response of a statistical mechanical model of two-component superfluid with a nondissipative drag interaction as the system undergoes a transition into a paired superfluid phase at finite temperature. The transition manifests itself in a change of (i) vortex-lattice symmetry and (ii) nature of the vortex state. Instead of a vortex lattice, the system forms a highly disordered tangle which constantly undergoes merger and reconnecting processes involving different types of vortices with a "hidden" breakdown of translation symmetry.

DOI: 10.1103/PhysRevB.78.144510 PACS number(s): 67.10.−j, 03.75.Hh, 03.75.Mn, 67.90.+z

I. INTRODUCTION

Recently, there has been increased interest in so-called "paired" states of superfluids (and also related counter-flow states) where pairing results from proliferation of *composite* topological defects in various physical contexts.[1–6] The mechanism can be outlined as follows. In certain systems, the energetically cheapest defects that proliferate under the influence of thermal fluctuations or applied external field are not the simplest vortex loops, rather, they are composite ones. That is, they have phase winding in several components of the order parameter, but nonetheless they lack topological charge in some sector of the model. Consequently, their proliferation does not restore symmetry completely. Broken symmetry may remain in, e.g., the sum of the phases of the order-parameter components, and the resulting state is frequently called a paired superfluid. Since the origin of pairing in this case is an entropy-driven formation of a tangle of composite topological defects, one encounters an unusual situation in which a system forms paired states as a consequence of heating. Thus, in what follows we will refer to this state as a thermally paired superfluid (TPS) to distinguish it from a conventional pairing mechanism.

Today, the experimentally most feasible system, within which to study TPS, appears to be multicomponent Bose-Einstein condensates. Here, TPS can arise[2,6] due to a current-current (Andreev-Bashkin[7]) interaction, which can be tuned in an especially wide range for bosons in optical lattices.[4] Questions therefore arise as to how the transition into a TPS alters the rotational response of the system and what are its experimental signatures. In this paper, we address this by studying a model of a mixture of two superfluids with a dissipationless drag in the London approximation, i.e., density fluctuations of the superfluid condensate components are neglected.

II. MODEL

The model is given by[6,7]

$$F=\frac{1}{2}\left\{\sum_{i=1,2} m_i n_i\left(\frac{\hbar\nabla\theta_i}{m_i}-\mathbf{\Theta}\right)^2 - \sqrt{m_1 m_2}\,n_d\left(\frac{\hbar\nabla\theta_1}{m_1}-\frac{\hbar\nabla\theta_2}{m_2}\right)^2\right\}, \tag{1}$$

where θ_i, n_i, and m_i are the phases, densities, and masses of the condensates, respectively, the angular frequency is given by $\mathbf{\Omega}=\nabla\times\mathbf{\Theta}$, while n_d controls the density of one component dragged by the other. The central feature of the model is that for significantly strong drag n_d the composite vortices with phase winding in both components ($\Delta\theta_1=2\pi,\Delta\theta_2=-2\pi$) [in what follows denoted by (1,−1)] become the energetically cheapest to excite and are the easiest objects of a thermal fluctuation-driven proliferation.[2,4,6] The resulting phase is well described by separating out the sector of the model unaffected by proliferation of composite vortices. Without rotation, the accuracy of this procedure was numerically checked in various regimes in Ref. 6. The Hamiltonian reads, after separation of variables,

$$F=\frac{1}{2}\left\{\left(\frac{\frac{n_1 n_2}{m_1 m_2}-\frac{n_d}{\sqrt{m_1 m_2}}\left(\frac{n_1}{m_2}+\frac{n_2}{m_1}\right)}{\frac{n_1}{m_1}+\frac{n_2}{m_2}-\sqrt{m_1 m_2}(m_1^{-1}+m_2^{-1})^2 n_d}\right)(\hbar\nabla\theta_1+\hbar\nabla\theta_2-(m_1+m_2)\mathbf{\Theta})^2+\left[\frac{n_1}{m_1}+\frac{n_2}{m_2}-\sqrt{m_1 m_2}(m_1^{-1}+m_2^{-1})^2 n_d\right]^{-1} \times\left[\left(\frac{n_1-n_d\frac{m_1+m_2}{\sqrt{m_1 m_2}}}{m_1}\right)(\hbar\nabla\theta_1-m_1\mathbf{\Theta})-\left(\frac{n_2-n_d\frac{m_1+m_2}{\sqrt{m_1 m_2}}}{m_2}\right)(\hbar\nabla\theta_2-m_2\mathbf{\Theta})\right]^2\right\}, \tag{2}$$

where the first term represents the part of the model unaffected by proliferation of (1,–1) vortices. In what follows, we consider the case $m_1=m_2=1$ and $n_1=n_2=\rho$ and $n_d=\rho_d$ in units where $\hbar=1$, namely,

$$F=\frac{\rho}{4}[\nabla(\theta_1+\theta_2)-2\mathbf{\Theta}]^2+\frac{\rho-2\rho_d}{4}[\nabla(\theta_1-\theta_2)]^2. \quad (3)$$

In the absence of rotation, the model [Eq. (3)] has three different phases. (i) At low drag and low temperature, there is a phase with broken $U(1)\times U(1)$ symmetry. (ii) At high temperatures there is a fully symmetric phase. (iii) At $\rho_d>0$, there is a phase with broken $U(1)$ symmetry only in the phase sum: This is the TPS. The phase diagram was studied in the J-current representation in Ref, 2 and, in terms of proliferation of vortex loops in the Villain model, in Ref. 6.

In this work, we address the question of the physics of this system when it is subjected to rotation. To this end, we have performed large scale Monte Carlo (MC) computations on Eq. (3) following the procedures of Ref. 6. Rotation is accounted for by choosing $\mathbf{\Theta}=(0,2\pi fx,0)$, where f is the number of rotation-induced vortices per plaquette in the xy plane. Our free energy is a function of the ratios of stiffnesses to temperature. Thus, we explore the phase diagram in terms of these dimensionless ratios, i.e., by absorbing the temperature in ρ and ρ_d. Thus, low values of ρ and ρ_d amount to high temperatures and vice versa. In these standard units and in the discretization scheme using the Villain approximation,

$$V_{i,\mu}=-\beta^{-1}\ln\Bigg\{\sum_{n_{i,\mu}^{(1)},n_{2i,\mu}^{(2)}}\exp-\frac{\beta}{2}\{\rho_1(\Delta_\mu\theta_{1,i}-2\pi n_{i,\mu}^{(1)})^2+\rho_2(\Delta_\mu\theta_{2,i}-2\pi n_{i,\mu}^{(2)})^2-\rho_d[\Delta_\mu(\theta_{1,i}-\theta_{2,i})-2\pi(n_{1,i}^{(1)}-n_{2,i}^{(2)})]^2\}\Bigg\}, \quad (4)$$

where $H_V=\Sigma_{i,\mu}V_{i,\mu}$. In Eq. (4), the fields $n_{i,\mu}^{(1)}$ and $n_{i,\mu}^{(2)}$ are integer-valued auxiliary fields that are summed over in the partition function, such that the action is 2π periodic in the phase fields $\theta_{1,i}$ and $\theta_{2,i}$ and Δ_μ denotes a lattice derivative in the μ direction. The single-component XY model in the Villain approximation has a critical stiffness $\rho_c\approx 0.33$.[8] We have considered cubic numerical grids, with periodic boundary conditions, of size L^3 with $L=64$ and 128. Throughout, we have a filling fraction $f=1/64$. For each coupling we have used 5×10^5 sweeps over the entire grid for thermalization and then used 1×10^6 sweeps for calculating averages.

In the limit $\rho_d\to 0$, the system tends toward two decoupled superfluids for which our simulations recover the standard triangular vortex-lattice forming in response to rotation. Already for a drag ρ_d as low as $\rho_d\approx 0.08$, the energetically most favorable vortex ordering becomes square vortex lattices for each of the components. These lattices are shifted with respect to each other half a lattice spacing in the x and y directions. This effect, arising in this hydrodynamic model with current-current interactions, has a counterpart in a system with a different type of interaction. Namely, square lattices are also known to appear in two-component condensates with density-density interaction.[9] Below, we study vortex matter with further increased drag and temperature by (i) inspection of three-dimensional (3D) snapshots of typical vortex configuration, (ii) calculating structure factors, and (iii) by calculating the quantity $\tilde{\nu}^i(\boldsymbol{r}_\perp)$ representing real-space averages over various numbers of MC sweeps of the vorticity integrated along the z direction defined as

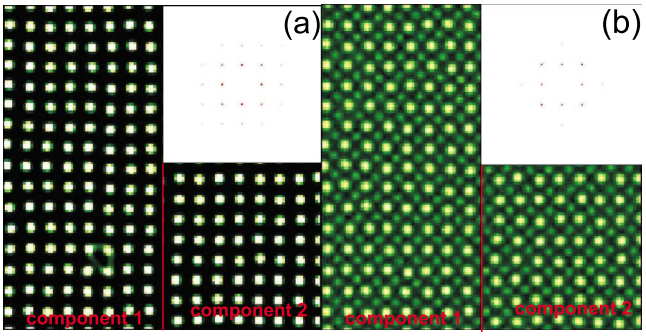

FIG. 1. (Color online) The average vortex positions in xy plane integrated along the z direction and averaged over every 100th of a total of 1×10^6 MC sweeps $[\tilde{\nu}^1(\boldsymbol{r}_\perp)]$. Here $\rho=0.924$ and $\rho_d=0.17$ in (a) and $\rho_d=0.37$ in (b). The brighter green color shows higher probability to find a vortex segment directed along the rotation axis. The left part of each panel shows vortices with phase winding in component 1 $\tilde{\nu}^1(\boldsymbol{r}_\perp)$, while the right part is that for the component 2 $\tilde{\nu}^2(\boldsymbol{r}_\perp)$. The lattices of the two components are displaced a half period in both directions. The inset shows the corresponding $\boldsymbol{k}$-space structure factor.

$$\tilde{\nu}^i(\boldsymbol{r}_\perp)=\left\langle\frac{1}{L_z}\sum_z\nu_z^i(\boldsymbol{r}_\perp,z)\right\rangle, \quad (5)$$

where $\nu_z^i(\boldsymbol{r}_\perp,z)$ is the vorticity of component i along the z direction at $\boldsymbol{r}=(x,y,z)$ and $\boldsymbol{r}_\perp=(x,y)$, $\langle\cdot\rangle$ denotes MC averaging. It is important to note that when $\tilde{\nu}^i(\boldsymbol{r}_\perp)$ shows a lattice ordering, although it signals a particular rotational response, it does *not* necessarily imply a vortex state visible in z-axis density averages. This is so because the MC and z axis averages in $\tilde{\nu}^i(\boldsymbol{r}_\perp)$ are taken over vorticity but not over a density. Vortex segments with opposite phase windings cancel each others vorticity in these averages.

In the low-drag low-temperature regime the quantity $\tilde{\nu}^i(\boldsymbol{r}_\perp)$ show peaks corresponding to a square lattice. At stronger drag, there appear weak intensity peaks in the *center of the plaquettes* for each of the components; cf. Fig. 1. This means that an increased drag and temperature creates a fluctuating vortex background such that there is an increased probability to find a segment of a vortex directed along the z direction and situated in the center of plaquettes of the square vortex lattice [Fig. 1]. In addition, the higher-order Bragg peaks disappear from the $\boldsymbol{k}$-space structure factor

$$S^{(i)}(\boldsymbol{k}_\perp)=\left|\frac{1}{L_xL_yL_zf}\sum_{\boldsymbol{r}_\perp,z}\nu_z^i(\boldsymbol{r}_\perp,z)e^{-i\boldsymbol{r}_\perp\boldsymbol{k}_\perp}\right|^2. \quad (6)$$

With increasing temperature, equivalently decreasing ρ, the intensity of new peaks in the quantity $\tilde{\nu}^i(\boldsymbol{r}_\perp)$ grows at sufficiently large ρ_d. Eventually, we observe a discontinuous

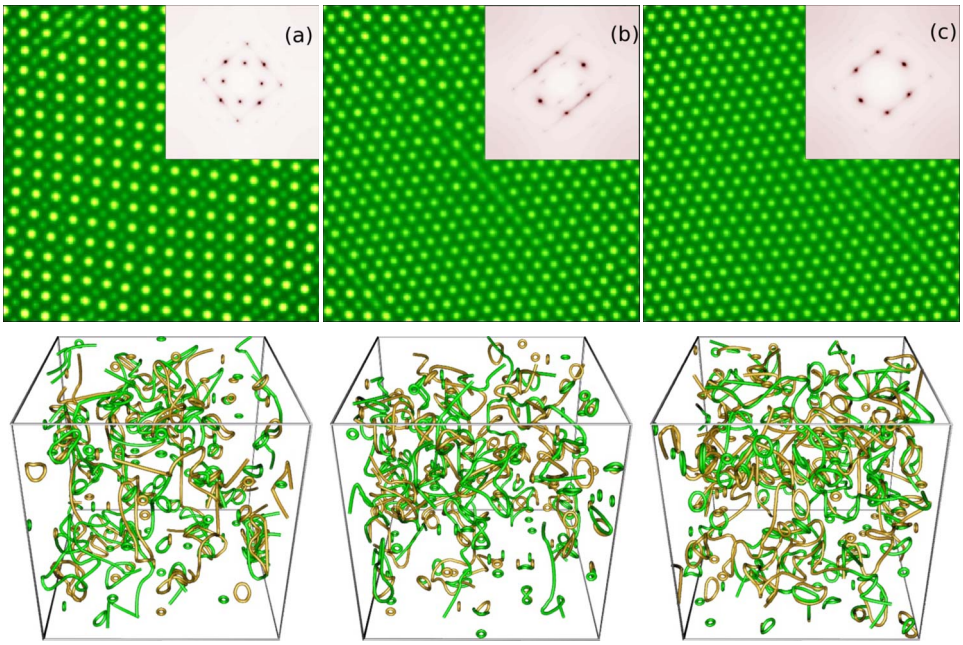

FIG. 2. (Color online) The upper row shows the xy position of component 1 vortices integrated along the z direction, $\tilde{\nu}^1(\boldsymbol{r}_\perp)$, averaged over every 100th of a total of 1.0×10^6 MC sweeps. (a) $\rho=0.984$, (b) $\rho=0.982$, (c) $\rho=0.980$, and $\rho_d=0.4$ in all panels. The inset shows the corresponding $\boldsymbol{k}$-space structure factor $S^1(\boldsymbol{k}_\perp)$. The bottom row shows typical 3D snapshots of the vortex configuration of a $16\times16\times16$ segment of the simulated system. The green and yellow colors represent vortices in different components. The figure shows the transition from a square lattice structure (leftmost column) to a triangular lattice structure (rightmost column). The middle column shows coexistence of a triangular and square lattice. The square lattice is seen in the left top and bottom corner of the panel (b); it is also possible to see a square structure inside the hexagonal structure in the $\boldsymbol{k}$-space inset. For visualizing the 3D snapshots, the vortex diameter is chosen to be 0.1 of the numerical grid spacing. Sharp bends arising at the scales of numerical grid spacing are smoothed by spline interpolation. For animations, see Ref. 10.

phase transition to a state with domains where the secondary real-space vortex position peaks have intensities equal to the primary peaks. In these domains, the lattice symmetry also changes from square to triangular, and the real-space position averages for each component become identical, i.e., $\tilde{\nu}^1(\boldsymbol{r}_\perp) \approx \tilde{\nu}^2(\boldsymbol{r}_\perp)$. These triangular lattice domains coexist with domains of square high-intensity lattices with a weaker intensity square sublattice, where $\tilde{\nu}^1(\boldsymbol{r}_\perp)$ is approximately the same as $\tilde{\nu}^2(\boldsymbol{r}_\perp)$, but shifted a half-lattice spacing in x and y directions. This is seen by comparing panels (a) and (b) in Fig. 2.

With further increase in temperature, the triangular lattice domains grow until $\tilde{\nu}^1(\boldsymbol{r}_\perp)$ and $\tilde{\nu}^2(\boldsymbol{r}_\perp)$ form identical essentially perfect triangular lattices which precisely coincide in space; cf. panels (c) of Fig. 3. Note also that now $\tilde{\nu}^j(\boldsymbol{r}_\perp)$ has twice as high number of vortex positions as the low-drag low-temperature case.

Figure 2 also shows snapshots of typical vortex configurations arising in these states. Even in the state with $U(1)\times U(1)$ symmetry and square lattice with relatively weak sublattice intensity peaks in $\tilde{\nu}^j(\boldsymbol{r}_\perp)$, it is not obvious from a typical snapshot that the system features a vortex lattice

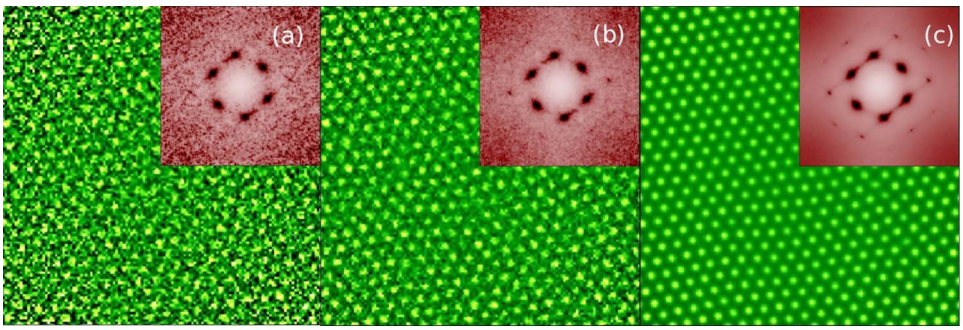

FIG. 3. (Color online) Panel (a) is a typical snapshot of $\tilde{\nu}^1(\boldsymbol{r}_\perp)$ with the corresponding $\boldsymbol{k}$-space structure factor as inset, while panel (b) is the corresponding quantity averaged over five different configurations (100 MC sweeps are used to obtain a new configuration) while in panel (c) the quantity is averaged over 1000 different configurations. We see that one needs to average over several configurations before a triangular lattice is clearly visible in $\tilde{\nu}^j$. The computations were done for $\rho=0.98$ and $\rho_d=0.4$.

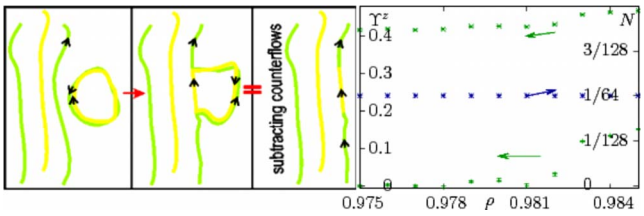

FIG. 4. (Color online) Left panel illustrates how a segment of a rotation-induced vortex line effectively can change color via merger with a thermally excited composite (1,−1) vortex loop. The process is responsible for, e.g., the appearance of sublattice peaks in $\tilde{\nu}(\boldsymbol{r}_\perp)$. Right panel shows that when the system undergoes a transition from square to triangular vortex lattice, the helicity modulus for the $(\theta_1 - \theta_2)$ sector Υ_- goes to zero, while the helicity modulus for component 1 Υ_1 stays finite (left axis). Also, it is seen that in spite of vortex number doubling in the quantity $\tilde{\nu}(\boldsymbol{r}_\perp)$, the number of z-directed rotation-induced vortex segments is constant (right axis: blue crosses). N is the number density of z-directed vortices.

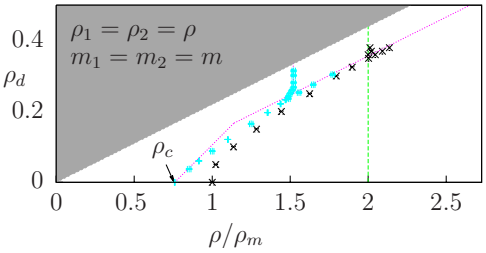

FIG. 5. (Color online) Phase diagram of the model [Eq. (1)] with and without rotation. Dotted lines and blue crosses are obtained from the analytical estimates and numerical results from Ref. 6. Black crosses are obtained in the current case of rotating system from the vanishing of the peaks of structure function at primary reciprocal-lattice vectors of the rotation-induced vortex lattice, which signals symmetry restoration.

which breaks translational symmetry. Moreover, it is impossible to see vortex lattices in any snapshots corresponding to the case when statistical averaging produces nearly perfect triangular lattice. Thus, we will use the term "hidden vortex lattice" (HVL) for this case. In Fig. 3, we show $\tilde{\nu}(\boldsymbol{r}_\perp)$ averaged over a different number of MC snapshots. In the case of triangular HVL, in contrast to the low-drag low-temperature case, averaging over a small number of MC snapshots shows no vortex lattice in real-space images. As seen from 3D snapshots, the effect should be stronger for density averages, i.e., averages performed over vortex-core positions instead of vorticity average of z-axis directed vortex and antivortex segments, represented by $\tilde{\nu}(\boldsymbol{r}_\perp)$.

The evolution of vortex matter with increasing temperature at significantly strong drag can be described as follows. Topologically, the increase in drag makes composite defects (1,−1) with energy $\sim\rho-2\rho_d$ the easiest objects to proliferate. The thermally generated composite (1,−1) vortex loops interact with the rotation-induced lattice through processes schematically illustrated in Fig. 4. For instance, a rotation-induced (0,1) vortex line can absorb a segment of a thermally created (1,−1) vortex loop. This changes the "color" of a segment of the rotation-induced line. Subtracting all counterflow segments [i.e., co-centered counter-directed vortices (1,−1)], which are not directly relevant to rotational response, shows that this process leads to a rotation-induced vortex lattice where the vortex lines comprising the lattice will have randomly alternating and thermally fluctuating colors. Indeed, when the number of thermally induced (1,−1) loops is low, each sublattice at any moment acquires only a small number of segments of vortices of another color via rare merger processes with thermally excited composite vortices. This is the origin of the weak sublattice intensity peaks appearing in the centers of each plaquette discussed above. At sufficiently strong drag the system should undergo a transition to the TPS via proliferation of (1,−1) vortices. In the TPS, the remaining broken $U(1)$ symmetry in the phase sum still allows the system to form rotation-induced lattices of individual vortices, but the individual vortices (1,0) and (0,1) will constantly absorb and emit (1,−1) vortex loops. Thus, one cannot attribute a specific color to them. In this state the system only has one type of color-indefinite topological defect, and the spatially and MC-averaged images $\tilde{\nu}(\boldsymbol{r}_\perp)$ display a triangular lattice. Even though the averaged real-space images show a doubled number of vortices as seen in Fig. 3, Fig. 4 illustrates that in our simulations the total number of z components of the elementary segments of rotation-induced vortices does not change. In snapshots, every rotation-induced vortex line on average consists of 50% green segments and 50% yellow segments. Overall, the system in this state is in a disordered vortex tangle state which is continuously undergoing merger processes between composite and individual vortices. The breakdown of spatial symmetry transpires only after spatial and MC averaging.

We now discuss quantitatively the influence of rotation for a given vortex density, on the phase diagram of the system. Figure 5 shows the phase diagrams of the model in the Villain approximation, both without rotation[6] and with rotation. In the zero-drag limit the broken-symmetry domain shrinks most significantly since under rotation the symmetry is now restored by lattice melting rather than vortex-loop proliferation. On the other hand, in the strong-drag limit an opposite situation arises. Namely, the transition from $U(1) \times U(1)$ to $U(1)$ TPS state is governed by composite vortices and for strong enough drag, the transition is almost unaffected by rotation-induced lattice of individual vortices. However, the transition from TPS to a fully symmetric state is strongly affected by rotation because it is dominated by vortex-lattice melting rather than vortex-loop proliferation. Note also that the stiffness at this transition is independent of ρ_d and is exactly twice the critical stiffness of the phase transition in the zero-drag limit. This demonstrates the accuracy of the separation of variables argument in Ref. 6 in case of a rotating system.

III. CONCLUSIONS

In conclusion, we have studied the rotational response of two superfluids with current-current (drag) interaction. At very low temperatures, the drag effect results in the formation of vortex lattices with square symmetry in response to rotation. At moderate temperatures, there appears a statistical

vorticity buildup in the form of a weak square sublattice. With further elevation of the temperature the system undergoes a transition to a TPS which we find is accompanied by a melting of the square lattice into a triangular one. The new triangular lattice breaks translation symmetry in a statistical sense. Snapshots of this state reveal a highly entangled vortex state. We stress that the quantities which we use, namely, $\vec{v}^i(\boldsymbol{r}_\perp)$ and $S^i(\boldsymbol{k})$, measure averaged vorticity and do not necessarily imply detectable breakdown of translation symmetry in density measurements. This might have experimental implications. There might be regimes where density snapshots may not display vortex lattices in the TPS even though the system may have perfectly triangular HVL from the point of view of the above quantities which measure averaged vorticity. It might, however, be possible in principle to detect HVL in interference experiments. Furthermore, in a certain sense a counterpart of some of the phenomena discussed above may be visible in the density profile of quasi-two-dimensional (2D) systems. There, in the regime of strong drag, the composite $(1,-1)$ vortices undergo a Berezinskii-Kosterlitz-Thouless transition at $(\rho/2-\rho_d)=\pi/4$ while the system retains the order in the phase sum for $\rho/2>\pi/2$. Under rotation, they can be expected to display a vortex lattice of individual vortices coexisting with a liquid state of thermally excited composite vortices and antivortices. Finally, we remark that the previous studies of the effect of a presence of a trap on thermally fluctuating vortices in single-component hydrodynamic model[11] suggest that a density variation in a trapped two-component condensate may produce a situation where several of the above states may be simultaneously present at different distances from the center of the trap.

ACKNOWLEDGMENTS

This work was supported by the Norwegian Research Council with Grants No. 158518/431, No. 158547/431 (NANOMAT), and No. 167498/V30 (STORFORSK).

[1] E. Babaev, Nucl. Phys. B **686**, 397 (2004); E. Babaev, A. Sudbø, and N. W. Ashcroft, Nature (London) **431**, 666 (2004); J. Smiseth, E. Smørgrav, E. Babaev, and A. Sudbø, Phys. Rev. B **71**, 214509 (2005).

[2] A. B. Kuklov and B. V. Svistunov, Phys. Rev. Lett. **90**, 100401 (2003); A. Kuklov, N. Prokofev, and B. Svistunov, *ibid.* **93**, 230402 (2004); A. Kuklov, N. Prokof'ev, and B. Svistunov, *ibid.* **92**, 030403 (2004); A. B. Kuklov, N. Prokof'ev, B. Svistunov, and M. Troyer, Ann. Phys. (N.Y.) **321**, 1602 (2006).

[3] D. Podolsky, S. Chandrasekharan, and A. Vishwanath, arXiv:0707.0695 (unpublished); L. Mathey, A. Polkovnikov, and A. H. Castro Neto, Europhys. Lett. **81**, 10008 (2008).

[4] V. M. Kaurov, A. B. Kuklov, and A. E. Meyerovich, Phys. Rev. Lett. **95**, 090403 (2005).

[5] A. B. Kuklov, M. Matsumoto, N. V. Prokof'ev, B. V. Svistunov, and M. Troyer, Phys. Rev. Lett. **101**, 050405 (2008); O. Motrunich and A. Vishwanath, arXiv:0805.1494 (unpublished).

[6] E. K. Dahl, E. Babaev, S. Kragset, and A. Sudbø, Phys. Rev. B **77**, 144519 (2008).

[7] A. F. Andreev and E. Bashkin, Sov. Phys. JETP **42**, 164 (1975); D. V. Fil and S. I. Shevchenko, Phys. Rev. A **72**, 013616 (2005).

[8] A. K. Nguyen and A. Sudbø, Phys. Rev. B **57**, 3123 (1998).

[9] E. J. Mueller and T.-L. Ho, Phys. Rev. Lett. **88**, 180403 (2002); V. Schweikhard, I. Coddington, P. Engels, S. Tung, and E. A. Cornell, *ibid.* **93**, 210403 (2004).

[10] The evolution of vortex matter at $\rho_d=0.4$ when ρ is decreasing from 1.5 to 0.85. The transition to "hidden" triangular lattice occurs at 00:26, followed by a transition to a vortex liquid at 00:31. See the http://www.phys.ntnu.no/super/gfx/becvortices.mp4

[11] S. Kragset, E. Babaev, and A. Sudbø, Phys. Rev. Lett. **97**, 170403 (2006); Phys. Rev. A **77**, 043605 (2008).